RESEARCH ARTICLE | JULY 18 2025

Influence of carrier density and disorder on the quantum Hall plateau widths in epitaxial graphene

Ignacio Figueruelo-Campanero ; Yuriko Baba ; Alejandro Jimeno-Pozo ; Julia García-Pérez ; Elvira M. González ; Rodolfo Miranda ; Francisco Guinea ; Enrique Cánovas ; Daniel Granados ; Pierre A. Pantaleón ; Pablo Burset ; Mariela Menghini

APL Mater. 13, 071119 (2025)
https://doi.org/10.1063/5.0279212

Influence of carrier density and disorder on the quantum Hall plateau widths in epitaxial graphene

Cite as: APL Mater. 13, 071119 (2025); doi: 10.1063/5.0279212
Submitted: 6 May 2025 • Accepted: 26 June 2025 •
Published Online: 18 July 2025

Ignacio Figueruelo-Campanero,[1,2,a)] Yuriko Baba,[3,4,a)] Alejandro Jimeno-Pozo,[1] Julia García-Pérez,[1] Elvira M. González,[1,2] Rodolfo Miranda,[1,5,6] Francisco Guinea,[1,7] Enrique Cánovas,[1] Daniel Granados,[1] Pierre A. Pantaleón,[1] Pablo Burset,[3,4,6] and Mariela Menghini[1,a)]

AFFILIATIONS

[1] IMDEA Nanociencia, Cantoblanco, 28049 Madrid, Spain
[2] Facultad Ciencias Físicas, Universidad Complutense de Madrid, 28040 Madrid, Spain
[3] Departamento de Física Teórica de la Materia Condensada, Universidad Autónoma de Madrid, 28049 Madrid, Spain
[4] Condensed Matter Physics Center (IFIMAC), Universidad Autónoma de Madrid, 28049 Madrid, Spain
[5] Departamento de Física de la Materia Condensada, Universidad Autónoma de Madrid, 28049 Madrid, Spain
[6] Instituto Nicolás Cabrera, Universidad Autónoma de Madrid, 28049 Madrid, Spain
[7] Donostia International Physics Center, Paseo Manuel de Lardizábal 4, 20018 San Sebastián, Spain

[a)] **Authors to whom correspondence should be addressed:** ignacio.figueruelo@imdea.org; yuriko.baba@uam.es; and mariela.menghini@imdea.org

ABSTRACT

The half-integer quantum Hall effect in graphene, characterized by the quantization of Hall resistivity as a function of applied magnetic field, offers opportunities for advancements in quantum metrology and the understanding of topological quantum states. While the role of disorder in stabilizing quantum Hall plateaus (QHPs) is widely recognized, the precise interplay between the plateaus' width, disorder, mobility, and carrier density remains less explored. In this work, we investigate the width of the $\nu = 6$ QHP in epitaxial graphene, focusing on two distinct regions of the device with markedly different electronic mobilities. Depending on the storage conditions, it is possible to modify the carrier density of graphene QHE devices and consequently increase or reduce the mobility. Our experiments reveal mobility variations of up to 200% from their initial value. In particular, the sample storage time and ambient conditions also cause noticeable changes in the positions and extension of the QHPs. Our results show that the QHP extension for $\nu = 6$ differs significantly between the two regions, influenced by both mobility and disorder, rather than solely by carrier density. Transport simulations based on the Landauer–Büttiker formalism with Anderson disorder in a scaled model reveal the critical role of impurities in shaping graphene transport properties, defining the extension of the QHPs. This study provides valuable insights into the interplay between mobility, disorder, and quantum transport in graphene systems.

I. INTRODUCTION

Over the last decade, graphene has been one of the most widely studied 2D van der Waals materials due to its unique properties and broad range of applications.[1–4] In particular, the relativistic electronic nature, Berry phase, together with its sub-lattice degree of freedom, leads to the appearance of the half-integer Quantum Hall Effect (HI-QHE) ($\rho_{xy} = h/[4 \times e^2(N + 1/2)] = h/(\nu e^2)$ for $N = 0, 1, \ldots$ or $\nu = 2, 6, \ldots$).[1,5,6] The possibility to induce this state in graphene opens a plethora of possibilities not only as a new platform to study the QHE or related phenomena[7–9] but also in the field of quantum metrology for the development of a quantum resistance standard based on graphene.[10–12]

The QHE has been extensively studied since its discovery, leading to promising research areas such as the role of *k-space* topology in condensed matter systems.[13,14] Theoretical efforts have been dedicated to the description of QHE characteristics reproducing experimental results at finite temperatures.[15–17] However, key aspects of the QHE remain unresolved, particularly the dependence of QHP width on parameters such as mobility, carrier density, and disorder,[18–21] especially in the case of large samples (hundreds of μm). While disorder is known to be essential for plateau formation by pinning the Fermi level in mobility gaps between Landau levels (LLs),[22] the precise role and extent of disorder in stabilizing QHPs are not yet fully understood, largely due to the experimental difficulty of controlling and characterizing it.

In this work, we study how mobility, disorder, and carrier density affect the $\nu = 6$ quantum Hall plateau (QHP) in an epitaxial graphene Hall bar. Using oxygen absorption/desorption to modulate carrier density without gating, we track changes in QHP width over time in two regions with different mobilities. These variations, up to 200% in mobility, reveal that QHP width depends not only on carrier density but also on disorder. Transport simulations using the Landauer–Büttiker formalism[23] with Anderson disorder support our findings, reproducing the observed trends.

This study provides a detailed examination of the interplay between mobility, disorder, and carrier density in stabilizing the QHPs in epitaxial graphene. These findings pave the way for future research into controlling QHPs through tailored disorder and mobility engineering, with potential implications for quantum device optimization and metrology applications.

II. EXPERIMENTAL METHODS

We used commercial single-layer graphene (SLG) grown epitaxially on 4H–SiC (0001) from Graphensic AB to fabricate Hall bars via a two-step optical lithography process. The studied device had a 100 μm channel width and length ($L = W$), ensuring $R_{xx} = \rho_{xx}$. It was mounted on a chip carrier inside a ^{4}He flow cryostat with a 9 T superconducting coil. Magnetotransport measurements were performed in a four-probe Delta configuration with a 1 μA current, probing different regions of the device [see Figs. 1(a) and 1(b)].

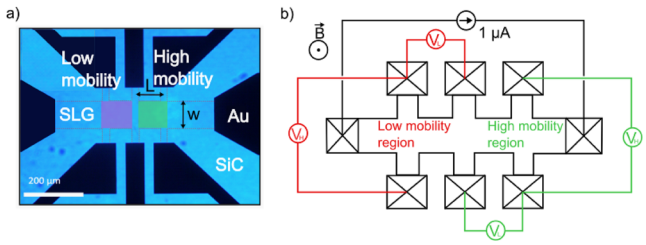

FIG. 1. (a) Optical microscope image of a $W = L = 100$ μm graphene Hall bridge. The SLG is indicated by the dotted area; blue contrast corresponds to the SiC substrate, and black regions correspond to the Ti/Au (10/90 nm) contacts. The green shaded area corresponds to the high mobility region in the SLG, and the red area to the low mobility one. (b) Schematics of the configuration used for the longitudinal (V_L) and Hall (V_H) voltage measurements presented in this work. The green (red) color corresponds to the configuration used to measure the high (low) mobility region.

Numerical calculations of the transport properties of a graphene Hall bar were performed considering a tight-binding model with nearest neighbor hopping (see Sec. 1 of the supplementary material for more details on the model employed). By including onsite Anderson disorder with strength ω_A, we studied the effect of impurities on the longitudinal and transversal graphene resistance. The resistance was obtained via the conductance matrix calculated within the Landauer–Büttiker framework employing Kwant.[23]

III. RESULTS AND DISCUSSION

A. Carrier density modulation and QHE under vacuum and air storage

The longitudinal and Hall resistances of graphene were characterized as a function of the applied magnetic field at different temperatures. The results at room temperature right after fabrication show a one order of magnitude difference in electron mobilities between the green and red regions marked in Fig. 1(a). This difference is attributed to possible residues during fabrication and/or intrinsic to the graphene/SiC sample (these are expected to be minimal due to the high quality of the commercial sample). To study graphene's electrical properties for different carrier concentrations, we analyzed the evolution of the longitudinal and Hall resistances under different storage conditions in the two different mobility regions, high mobility (HM) (green) and low mobility (LM) (red) [Fig. 1(a)]. As reported in previous studies,[24–31] the carrier density in epitaxial graphene can be tuned by adsorption or desorption of different types of molecules at the surface.

Adsorbed oxygen, among other molecules present in the atmosphere, can lead to a change in electron carrier density as it can act as an electron acceptor, decreasing the electron carrier concentration.[25,27] The results for the HM (LM) region as a function of vacuum storage (air storage) are presented in Fig. 2, top (bottom) panels. It is important to note that in our graphene Hall bar, the transport is dominated by electrons for all the data shown in this paper.

The graphene electronic properties are analyzed by extracting the carrier density and mobility as a function of temperature. First, the carrier density is obtained from the Hall resistivity, ρ_{xy}, at low magnetic fields, Fig. 2(a), following the Drude formalism $n = (d\rho_{xy}/dB)^{-1}/e$, where e is the electron charge and B is the applied magnetic field. For the HM region, the as-fabricated sample presents a carrier density of $5.1 \cdot 10^{11}$ cm^{-2} at 5 K (see Sec. 2 of the supplementary material for temperature dependences). The sample was kept in vacuum conditions ($\approx 10^{-3}$ mbar), and the carrier density evolution was studied as a function of the storage time.

The slope $d\rho_{xy}/dB$ at low magnetic fields decreases with storage time, meaning carrier density increases when the sample is stored in vacuum. The observed increase in n can be explained in terms of the removal of adsorbed molecules from the surface of graphene when the sample is kept longer in vacuum conditions. Wang *et al.*[32] have demonstrated the photochemical control of the concentration of adsorbed molecular oxygen in graphene using a UV laser. To confirm that the carrier modulation in our case is mainly driven by the desorption of oxygen molecules, UV laser annealing was done

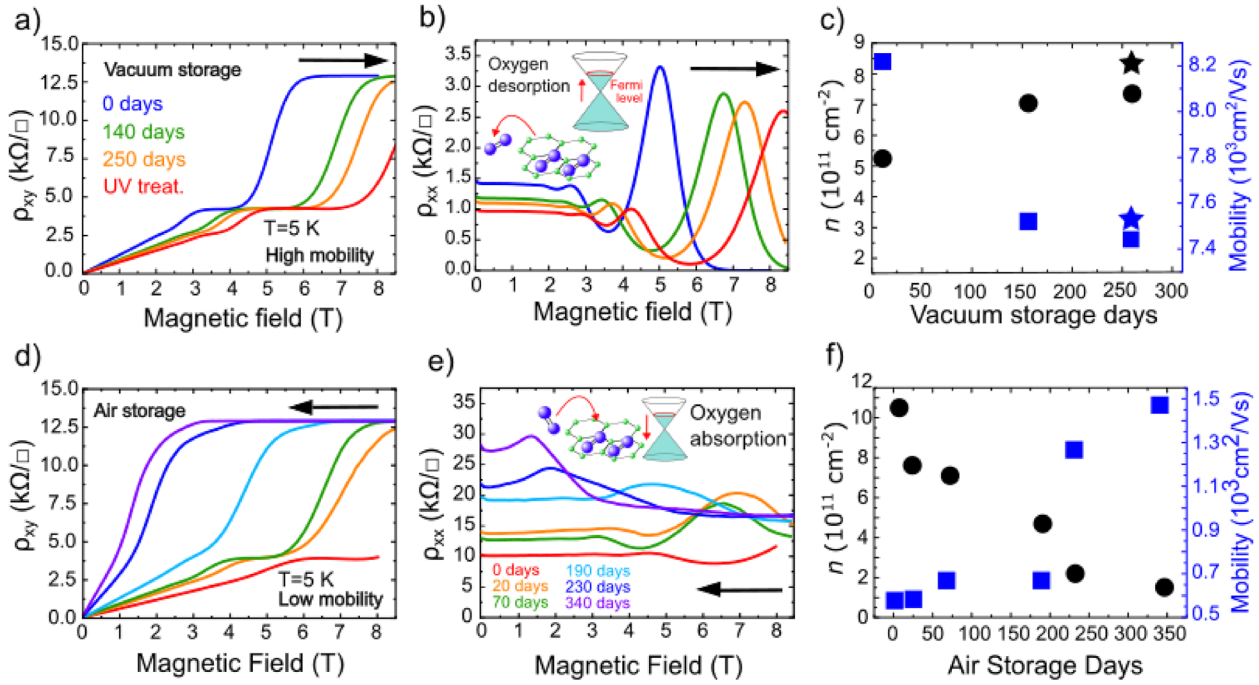

FIG. 2. High mobility region: (a) Hall resistivity and (b) longitudinal resistivity as a function of the applied magnetic field for different vacuum storage times and for the UV treatment (red line) at 5 K. (c) Evolution of carrier density (black circles) and mobility (blue squares) with vacuum storage time. Star shaped markers correspond to the UV treatment (387 nm, 5 s, 60 W/cm^{-2}). Low mobility region: (d) Hall resistivity and (e) longitudinal resistivity as a function of the magnetic field for different air storage times at 5 K. (f) Evolution of carrier density (black circles) and mobility (blue squares) with air storage time. The black arrows in [(a), (b), (d), and (e)] point in the direction of the shift in the Hall plateaus due to aging in each storage condition.

after 250 days of storage in vacuum. We illuminated the sample with a UV laser (387 nm) for 5 s with a fluence of 60 W/cm^2 to minimize heating effects. Immediately after UV treatment, the sample was mounted in the cryostat and measured. An increase in the carrier density of $\Delta n = 10^{11}$ cm^{-2} was observed [star shaped marker in Fig. 2(c)], suggesting that the modulation of carrier density for vacuum storage comes mostly from desorption of molecular oxygen.[32]

The electron mobility is extracted following the Drude formula: $\mu = (L/W)[en\rho_{xx}(B=0)]^{-1}$, using the carrier density previously obtained from the Hall resistivity slope and the values of the longitudinal resistivity at zero magnetic field ρ_{xx} (0), Fig. 2(b). The as-fabricated sample has a mobility of 8500 cm^2/Vs, in accordance with other epitaxial graphene reported in Ref. 28. We observe that as carrier density increases with vacuum storage time, this has a detrimental effect on the mobility, which decreases over time, reaching 87% of the starting value after 250 days. This effect has already been reported in previous works.[33–35]

In contrast, an increment of $\Delta\mu \approx 50$ cm^2/Vs in the mobility after the UV treatment was observed. In this case, the increase in carrier density accompanied by an increase in mobility could be attributed to thermal annealing effects due to laser heating.

In summary, a carrier density increase and a mobility reduction are observed with vacuum storage time. The observed variations in the mobility within the sample are driven by the modulations of carrier density.[36–39] In this case, when more oxygen adatoms are desorbed over time, more carriers are present in the sample, and the overall effect is to lower the mobility. This means that oxygen adatoms only play the role of modulating the carrier density and have a minor effect on the scattering times of the system (as we will discuss below, the scattering times do not change significantly as a function of storage time). This is reasonable, as molecular oxygen on graphene should be weakly bound via physisorption,[40,41] and thus, minimal changes are induced directly on the graphene lattice. Similar effects with vacuum storage and UV radiation are expected to occur in the LM region, as reversible modifications in carrier density and mobility with adsorption/desorption of molecular oxygen have been reported in low-mobility samples.[32]

For high enough magnetic fields, the system enters the QH regime. In the as-fabricated sample, we observe the appearance of plateaus $\nu = 6$ $(N = 1)$ around 3 T and $\nu = 2$ $(N = 0)$ around 6 T, and their corresponding Shubnikov de Haas (SdH) oscillations in the longitudinal resistivity ρ_{xx}; see Fig. 2(b). The effect of removing oxygen from the surface via vacuum storage is also observed in the location and extension of QHPs and SdH oscillations. As storage time increases (and thus carrier density), the position of SdH oscillations is shifted toward higher magnetic fields. This is expected as carrier density is increasing, and therefore a higher magnetic field is required to accommodate the gained extra carriers (electrons) due to increased degeneracy of the LLs (see Sec. 3 of the supplementary

material). In the case of UV treatment, the QHP $\nu = 2$ appears at magnetic fields beyond the largest magnetic field available in our setup (in agreement with a further increase in the carrier density). However, the plateau $\nu = 6$ is still visible, and even a glimpse of the plateau $\nu = 10$ can be discerned. In the LM region [red area in Fig. 1(a)], the initial carrier density, after the measurements in the HM region, was of the order of 10^{12} cm^{-2} and the mobility 640 cm^2/Vs. Notably, QHE was also stabilized in this region despite the difference in mobility of one order of magnitude; see Fig. 2(d). In this case, the high initial electron carrier concentration (red curve) does not allow the observation of the $\nu = 2$ plateau in the magnetic field range accessible in our experimental setup, but the plateau $\nu = 6$ is located at a field similar to that of the last measurement presented for the HM region (250 days in vacuum + UV). For this part of the study, we followed the evolution of graphene transport properties as the sample was kept in the air. As time passed, the electron density decreased due to the air exposure and consequently re-adsorption of oxygen molecules. An increase in the longitudinal resistance at zero magnetic field is also observed in these conditions; see Fig. 2(e).

The evolution of carrier density and mobility for this region as a function of time is summarized in Fig. 2(f). During air storage, the evolution of carrier density and mobility retraces back the behavior seen in the previous case. The exposure to air allows us to fully recover the initial carrier concentration present originally in the HM region and to go even below that value, down to $3 \cdot 10^{11}$ cm^{-2}. After 190 days in the air, the plateau $\nu = 2$ is established within the accessible field range, and after ~340 days, the quantization is observed by only applying 3 T [see Fig. 2(d)]. The corresponding longitudinal resistivities for the different storage times depicted in Fig. 2(e) show some modulation with the magnetic field corresponding to the SdH oscillations. Nevertheless, none of them shows the distinctive minima near zero resistance as it was observed in the HM region when entering the $\nu = 2$ QHP regime. The longitudinal resistivity in the QHE is modified according to the evolution of the density of states at the Fermi level with the applied magnetic field. When impurities are added to the system, the LLs start to widen, increasing the number of localized states in the mobility gap. At a certain point, this can lead to a finite longitudinal conduction by means of thermally activated or hopping transport mechanisms, thus reducing the expected quantized conductivity.[42]

B. Role of mobility, carrier density, and scattering time in the QHPs

We now discuss the relation between carrier density, mobility, and scattering time for the results presented in Sec. III A and their influence on the QHP extension. Figure 3(a) shows the behavior of mobility as a function of the carrier density for both HM and LM regions. As observed in Sec. III A, mobility is affected by the carrier density modulation during storage time. In both regions, mobility decreases as the carrier density increases. However, despite similar carrier densities being obtained during the experiments, the mobility values differ significantly between the HM and the LM regions, as shown in the inset in Fig. 3(a). This trend has been reported in previous works and aligns with various theoretical frameworks.[35,38,39]

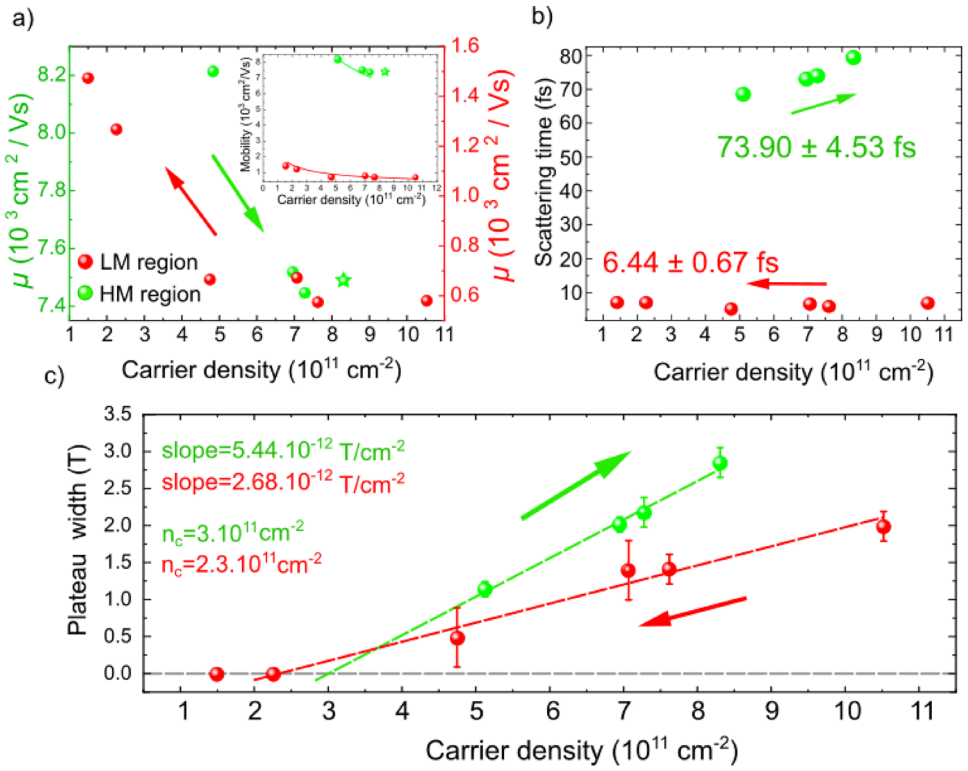

FIG. 3. (a) Characteristic mobility as a function of carrier density for the HM region (left axis) and the LM region (right axis). Inset: Same as main panel but using the same scale of mobility for both regions. The continuous lines correspond to a fitting using the model described in Ref. 35; see main text. (b) Scattering time evolution with carrier density for the HM and LM regions. The average scattering rate extracted for each region is shown. (c) QHP width for $\nu = 6$ for different carrier densities for the HM and LM regions. In both figures, the arrows indicate the direction of evolution of carrier density with time in each region. Dotted lines represent the linear fit for each region, with the corresponding values for the slope and intercept (n_c) indicated in the figure.

According to classical Drude's transport model, the mobility in graphene follows the relation $\mu(n) = \tau e v_F/(\sqrt{n\pi}\hbar)$, where v_F is the Fermi velocity and τ is the average scattering time, left as a constant parameter in Drude's original work.[43] This model captures the observed behavior where mobility is inversely proportional to carrier density ($\mu \propto 1/\sqrt{n}$). Moreover, within this model, the difference in mobility values can be attributed to variations in the scattering times between the two regions. The Drude model can be extended, as reported in the work of Gosling *et al.*,[35] using Boltzmann transport theory with Born approximation to lift the constraint of a constant scattering time. This dependence now results in a more general expression for mobility vs carrier density, as the scattering time is dependent on the carrier density $\tau(n)$. This gives a more general expression for mobility vs carrier density as $\mu(n) \propto n^{\beta}$, where the exponent β depends on the Fermi level position and the type of scatterers present in the system. In our case, we found that the exponents $\beta_{\mathrm{HM}} = -0.30$ and $\beta_{\mathrm{LM}} = -0.57$ fit reasonably well our experimental data; see the inset of Fig. 3(a).

To further analyze the dependence of the scattering time, we examine the evolution of this parameter with carrier density for both regions, Fig. 3(b). As shown, scattering time can slightly vary with the carrier density of the system. In the HM region, the scattering time increases with carrier density, whereas in the LM region, it remains nearly constant over the same range of carrier densities. As discussed in the work of Gosling *et al.*,[35] the scattering time can have different dependencies on the carrier density depending on the nature of the scatterers. An increase in the scattering time with carrier density could be due to long-range scatterers or, beyond the model, due to strong defect scattering.[44]

Similarly to mobility, the scattering time values differ significantly between the two regions by almost one order of magnitude, suggesting that carrier density alone does not fully determine this quantity. In fact, the scattering time is related to impurity density n_{imp} and strength, U_0[35] as $\tau \propto n_{\mathrm{imp}}^{-1}(A_{sr}U_0^2)^{-1}$, where A_{sr} is the effective cross section. As the scattering time presents minimal variations with carrier density in each experiment, we conclude that the mechanism relevant for the modulation of the carrier density, namely, the adsorption and desorption of molecular oxygen, alters minimally τ (and thus minimally changes n_{imp} and U_0), aside from their influence via carrier density modulation. This result is in accordance with the physisorption of oxygen molecules aforementioned, and therefore, the observed differences in scattering time can be primarily attributed to the impurities already present in the sample.

We estimate the difference in n_{imp} and U_0 between regions by applying the aforementioned approximation for τ in both regions. As both n_{imp} and U_0 are modifying the scattering time, it is not experimentally possible to disentangle the nature of the observed mobility variation differences in the studied sample. However, in our case, it is reasonable to consider that the types of scatterers present in both regions of the sample are similar and, thus, have comparable scattering strengths, $U_0|_{\mathrm{LM}} \approx U_0|_{\mathrm{HM}}$. Consequently, the primary factor contributing to the difference in mobility and scattering times between the two regions is likely the impurity density. An average scattering rate is extracted, obtaining a scattering rate of $\tau_{\mathrm{HM}} = 73.90 \pm 4.53$ fs and $\tau_{\mathrm{LM}} = 6.44 \pm 0.67$ fs for the HM and LM regions, respectively. Then, we can estimate the following relation for the impurity densities in both regions: $(n_{\mathrm{imp}}^{\mathrm{LM}})/(n_{\mathrm{imp}}^{\mathrm{HM}}) \propto \tau_{\mathrm{HM}}/\tau_{\mathrm{LM}} \approx 12$ (see Sec. 4 of the supplementary material).

We now discuss how the width of the QHPs evolves with the carrier density for the HM and LM regions. We focus on $\nu = 6$, since this is the only plateau that was fully observed for all storage times in the range of magnetic fields accessible in our experiments (see Sec. 5 of the supplementary material for the details about the plateau width definition). In Fig. 3(c), the plateau width for each region is presented as a function of the carrier density in the system. The plateau width shows a clear linear dependence on the carrier density, growing as the electron density increases for both regions (note that the time evolution is the opposite for each region, as indicated by the arrow directions in Fig. 3). For the HM region, the electron density increases with time, and so does the plateau extension, from an initial $\Delta B = 1$ T to almost triple after 300 days plus the UV treatment. In contrast, storage time reduces the number of carriers in the LM region, and the QHP for $\nu = 6$ shrinks from 2 T until disappearing at $n_c^{\mathrm{LM}} \approx 2.3 \cdot 10^{11}$ cm^{-2}. For comparison, the plateau in the HM region disappears at a larger critical carrier density of $n_c^{\mathrm{HM}} \approx 3 \cdot 10^{11}$ cm^{-2} (obtained by extrapolating the experimental points).

Even though both regions present similar carrier densities along different stages of storage, the measured QHP widths are different. The HM region displays, overall, broader plateaus than the LM one, suggesting that the main parameter that defines the width of the QHPs (aside from carrier density as explained before, through the LLs degeneracy) is the impurity density n_{imp} and their strength U_0. To obtain further microscopic insight on the impact of disorder and carrier density in the QHP width, we numerically compute the transport properties of a graphene Hall bar described by a scaled tight-binding model[45] (see Sec. 1 of the supplementary material). Disorder in the system is modeled by an Anderson on-site energy where ω_A quantifies the disorder strength (similar to U_0).[46] The Anderson model can qualitatively describe the effect of uncorrelated and short-range disorder in the samples without resorting to more sophisticated *ab initio* techniques. The results of the microscopic calculations, averaged over 100 disorder realizations (see the supplementary material), are reported in Fig. 4.

In Fig. 4(a), the transversal resistance R_{xy} is represented for three chemical potentials E_F as a function of the applied magnetic field B. The ideal cases without disorder are plotted with solid lines and show perfectly quantized plateaus with sharp transitions. The cases with Anderson disorder are represented with dashed lines, the shadowed areas corresponding to the standard deviation of the disorder realizations with respect to the mean value. A disordered potential landscape destroys the quantization near the edges of each plateau as the electrons can get from one side of the sample to the other by impurity localized states. As a result, there is a smooth transition between plateaus rather than the steps shown for the ideal case. The loss of the quantization between the plateaus also impacts the longitudinal resistance, represented in Fig. 4(b). In fact, R_{xx} develops large non-zero peaks for magnetic fields corresponding to the R_{xy} plateau transitions, experimentally corresponding to the SdH oscillations. The numerical calculations indicate that the plateaus shift toward higher magnetic fields when the chemical potential is increased, as already reported in Ref. 47 and in accordance with the increments in the carrier density observed in

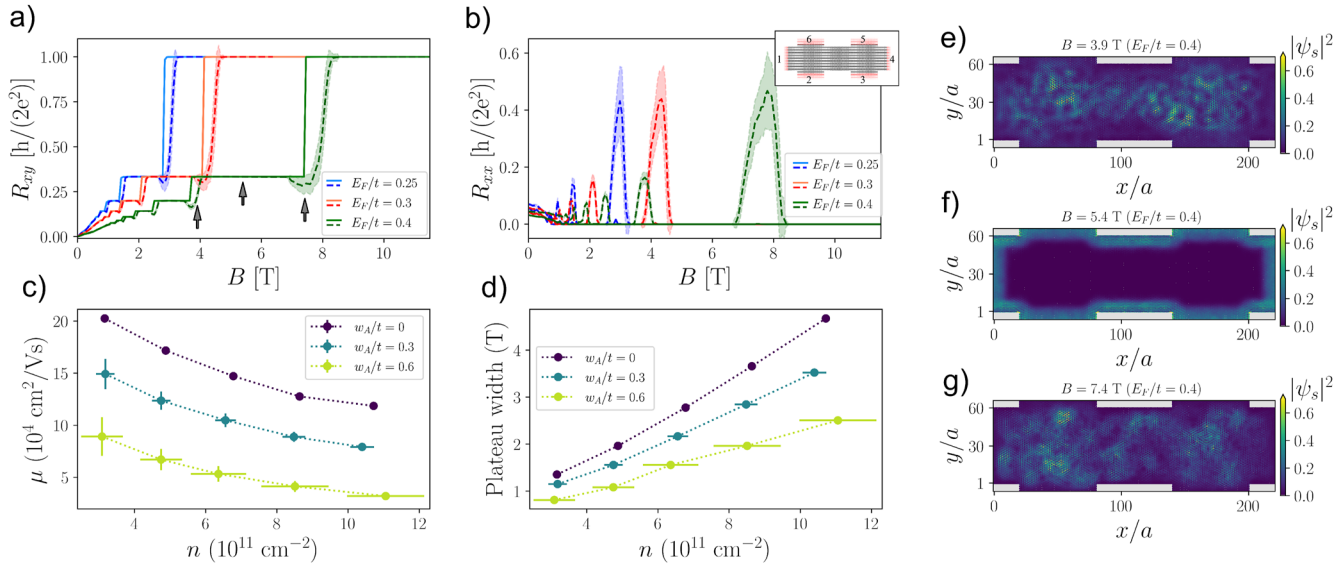

FIG. 4. (a) Transversal resistance R_{xy} as a function of the magnetic field B for three different values of the chemical potential E_F. The solid lines correspond to the case without disorder, and the dashed lines show the mean value of the resistance over 100 realizations for $\omega_A/t = 0.3$, with the shadowed areas indicating the standard deviation over the disorder realizations. (b) Longitudinal resistance for the same parameters as in (a). (c) Mobility μ and (d) plateau width as a function of carrier density n for $\nu = 6$ and three different disorder strengths (the error bars represent the propagation of the standard deviation of the disorder realizations). [(e)–(g)] Scattering wavefunction density distributions $|\psi_s|^2$ for three different magnetic fields indicated by arrows in (a).

the experimental data. The simulations are thus consistent with the experimental results for the HM vacuum stored (LM air stored) sample, where the carrier density increased (decreased) due to oxygen desorption (absorption).

Figure 4(c) shows the relation between mobility and carrier density from the numerical simulations. The case without disorder (purple dots) displays a Drude-like behavior in which the mobility is reduced with increasing the carrier density as $\mu \propto 1/\sqrt{n}$. The effect of disorder, quantified by the Anderson disorder potential ω_A, is to reduce the magnitude of the mobility. This reduction can be close to an order of magnitude at high carrier densities. The presence of disorder also induces a small change in the slope of the mobility–density ratio, which reduces slightly at higher disorder strength. The effect of disorder in our numerical simulations is thus consistent with the differences between HM and LM regions shown in Fig. 3(a) by associating the HM (LM) region with a higher (lower) w_A value. We now focus on the experimentally relevant plateau for the filling factor $\nu = 6$ and resistance $R_{xy} = R_0/3$, with $R_0 = h/(2\times 10^2)$. We characterize the plateau width by the quantity ΔB defined by the difference between the minimum and maximum value of the magnetic field where the standard deviation of the transversal resistance, $\sigma(R_{xy})$, is bigger than a given threshold $[\sigma(R_{xy}) > 10^{-3}R_0/3]$. For a fixed disorder strength in the system, ΔB increases with the carrier density n almost linearly at high densities; see Fig. 4(d). The presence of disorder reduces the plateau width for all carrier densities. At low carrier density, the calculations show a nonlinearity of the plateau width with the carrier density. Still, extrapolating from low or high carrier densities, we observe that the intercept (related to the critical carrier density observed in the experiments) increases with diminishing disorder strength. These calculations are consistent with the experimental observation of the narrowing of the plateau width with time for the LM region when stored in the air, as oxygen absorption reduces the carrier density. Conversely, in the vacuum-stored HM region, the carrier density increases, resulting in a broader plateau. Moreover, the differences in disorder between both regions provide an explanation for the observed overall differences in the plateau widths for the studied carrier density ranges. Therefore, our numerical calculations capture the experimental observation of an enlargement of the plateau width with increasing carrier density and a reduction of the quantized region due to an increase in disorder; see Figs. 3(b) and 4(d).

Finally, we analyze the microscopic effect of disorder on the electronic transport by plotting the density of the space-resolved scattering wavefunction for some relevant cases. The scattering wavefunction ψ_S is a valuable tool for examining the spatial distribution of the electronic density of the scattering states.[23,48] The scattering wavefunction density, defined as $|\psi_S|^2$, is plotted in Figs. 4(e)–4(g) for the three magnetic field values marked in Fig. 4(a) and for a disorder configuration corresponding to $\omega_A/t = 0.3$ and chemical potential $E_F/t = 0.4$. In panels (e) and (g), the magnetic field values considered correspond to a transition point between plateaus. Consequently, $|\psi_S|^2$ is affected by the landscape of the Anderson disorder potential and appears delocalized in the central part of the scattering region, indicating electron scattering from edge to edge, leading to non-quantized transversal resistance values. By contrast, Fig. 4(f) shows the density of the scattering wavefunction $|\psi_S|^2$ for a magnetic field corresponding to a perfectly quantized transversal resistance value. The density now peaks around the edges

of the sample, displaying a perfectly transmitting edge state that is resilient to the disorder.

IV. CONCLUSIONS

We have studied the evolution of the QHE characteristics in epitaxial graphene for different carrier densities and different storage conditions. By means of electrical transport measurements, we obtain the mobility and the carrier density for two different regions that differ strongly in their mobility. For the HM region, by storing the sample in vacuum, an increase in the carrier density was observed together with a major decrease in the mobility. The QHPs shift toward higher magnetic fields due to the LL degeneracy. By UV illumination, we can conclude that the induced changes are driven by molecular oxygen being desorbed from the surface with a consequent increase in the carrier density due to its electronegativity. For the LM region, the evolution of the carrier density and QHE characteristics was studied as the sample was kept in air. The results obtained showed that after around 350 days, the carrier density decreased almost by a factor of 10, the mobility increased up to 200% of the initial value, and the QHP shifted toward lower magnetic fields. Our experiments show that the difference in mobility and scattering time between the two studied regions can be attributed to different local impurity densities. From the QHE, we observe an increase in plateau width with increasing carrier density, attributed to larger energy spacing between LLs. Nevertheless, a difference in plateau width between the HM and LM regions was observed for similar carrier densities, indicating that the impurity density is a crucial parameter in defining the plateau width. Transport simulations based on a scaled tight-binding model for different disorder strengths show a similar relation between mobility and carrier density as in the experiments. The effect of the disorder strength in the simulations is to decrease the magnitude of mobility and plateau width, in agreement with the experimental results. Microscopically, the reduction in the plateau width is caused by edge to edge scattering enabled by impurities, destroying the perfect ballistic conductance.

This study contributes to the understanding of the effects of disorder in the QH regime in graphene. The observation of the evolution of QHP width for different carrier densities and their dependence on the disorder in the sample highlights the important role played by these parameters in the QH state. This is relevant not only for an in-depth understanding of this quantum state but also for applications of graphene, such as metrology, where disorder can play a major role in the development and engineering of future stable and reliable resistance standards operational in relaxed experimental conditions.

SUPPLEMENTARY MATERIAL

The supplementary material contains descriptions of the theoretical model for tight binding calculations and of the relation between scattering time and impurity concentration and strength. It also includes results on the evolution of carrier density and mobility with temperature for different storage times and the observed shifts of the QHP center with carrier density. Finally, the method used for the definition of QHPs and a summary of relevant parameters for the high mobility and low mobility regions are presented.

ACKNOWLEDGMENTS

We thank Ming-Hao Liu and Rafael A. Molina for their valuable discussions and Sergio Revuelta for his help with the UV radiation experiments. This work was supported by the Spanish Ministry for Science and Innovation (MCIN) under Project Nos. PGC2018-098613-B-C21 (SporQuMat), PID2021-122980OB-C52 (ECoSOx-ECLIPSE), and EMPIR 20FUN03 COMET project. IMDEA Nanociencia acknowledges the support from the "Severo Ochoa" Program for Centers of Excellence in R&D (Grant Nos. SEV-2016-0686 and CEX2020-001039-S). I.F.C. holds an FPI fellowship from AEI-MCIN (PRE2020-092625). Y.B. and P.B. acknowledge the support by the Spanish CM "Talento Program" Project Nos. 2019-T1/IND-14088 and 2023-5A/IND-28927, the Agencia Estatal de Investigación Project Nos. PID2020-117992GA-I00 and CNS2022-135950, and through the "María de Maeztu" Programme for Units of Excellence in R&D (CEX2023-001316-M). A.J.-P., F.G., and P.A.P. acknowledge the support from NOVMOMAT, Project No. PID2022-142162NB-I00 funded by MICIU/AEI/10.13039/501100011033 and by FEDER, UE, as well as the financial support through the (MAD2D-CM)-MRR MATERIALES AVANZADOS-IMDEA-NC. E.C. acknowledges the funding from the Spanish Project No. CNS2022-136203-Consolidación investigadora and TED2021-129624B-C44 .

AUTHOR DECLARATIONS

Conflict of Interest

The authors have no conflicts to disclose.

Author Contributions

Ignacio Figueruelo-Campanero: Conceptualization (lead); Data curation (lead); Formal analysis (lead); Investigation (lead); Methodology (lead); Validation (lead); Writing – original draft (lead); Writing – review & editing (lead). **Yuriko Baba**: Conceptualization (-lead); Data curation (lead); Formal analysis (lead); Investigation (lead); Methodology (lead); Validation (lead); Writing – original draft (equal); Writing – review & editing (equal). **Alejandro Jimeno-Pozo**: Formal analysis (supporting); Investigation (supporting); Methodology (supporting); Validation (supporting); Writing – review & editing (supporting). **Julia García-Pérez**: Investigation (supporting); Methodology (supporting); Writing – review & editing (supporting). **Elvira M. González**: Funding acquisition (supporting); Investigation (supporting); Methodology (supporting); Supervision (equal); Validation (supporting); Writing – review & editing (supporting). **Rodolfo Miranda**: Funding acquisition (lead); Investigation (supporting); Supervision (supporting); Writing – review & editing (supporting). **Francisco Guinea**: Formal analysis (supporting); Investigation (supporting); Writing – review & editing (supporting). **Enrique Cánovas**: Formal analysis (supporting); Funding acquisition (equal); Investigation (equal); Writing – review & editing (supporting). **Daniel Granados**: Investigation (equal); Methodology (equal); Supervision (supporting); Writing – review & editing (supporting). **Pierre A. Pantaleón**: Formal analysis (supporting); Investigation (supporting); Writing – review & editing (supporting). **Pablo Burset**: Conceptualization (equal); Data curation (equal); Formal analysis (equal); Investigation (equal); Methodology (equal); Supervision (equal); Writing –

original draft (equal); Writing – review & editing (equal). **Mariela Menghini**: Conceptualization (lead); Formal analysis (equal); Funding acquisition (lead); Investigation (equal); Methodology (supporting); Supervision (equal); Writing – original draft (lead); Writing – review & editing (lead).

DATA AVAILABILITY

The data that support the findings of this study are available from the corresponding author upon reasonable request.

REFERENCES

[1] K. S. Novoselov, A. K. Geim, S. V. Morozov, D. Jiang, M. I. Katsnelson, I. V. Grigorieva, S. V. Dubonos, and A. A. Firsov, "Two-dimensional gas of massless Dirac fermions in graphene," Nature **438**(7065), 197–200 (2005).

[2] A. H. Castro Neto, F. Guinea, N. M. R. Peres, K. S. Novoselov, and A. K. Geim, "The electronic properties of graphene," Rev. Mod. Phys. **81**(1), 109–162 (2009).

[3] A. K. Geim and K. S. Novoselov, "The rise of graphene," Nat. Mater. **6**(3), 183–191 (2007).

[4] K. S. Novoselov, V. I. Fal'ko, L. Colombo, P. R. Gellert, M. G. Schwab, and K. Kim, "A roadmap for graphene," Nature **490**(7419), 192–200 (2012).

[5] K. S. Novoselov, Z. Jiang, Y. Zhang, S. V. Morozov, H. L. Stormer, U. Zeitler, J. C. Maan, G. S. Boebinger, P. Kim, and A. K. Geim, "Room-temperature quantum Hall effect in graphene," Science **315**(5817), 1379 (2007).

[6] Y. Zhang, Y.-W. Tan, H. L. Stormer, and P. Kim, "Experimental observation of the quantum Hall effect and Berry's phase in graphene," Nature **438**(7065), 201–204 (2005).

[7] Z. Lu, T. Han, Y. Yao, A. P. Reddy, J. Yang, J. Seo, K. Watanabe, T. Taniguchi, L. Fu, and L. Ju, "Fractional quantum anomalous Hall effect in multilayer graphene," Nature **626**(8000), 759–764 (2024).

[8] K. I. Bolotin, F. Ghahari, M. D. Shulman, H. L. Stormer, and P. Kim, "Observation of the fractional quantum Hall effect in graphene," Nature **462**(7270), 196–199 (2009).

[9] C. L. Kane and E. J. Mele, "Quantum spin Hall effect in graphene," Phys. Rev. Lett. **95**(22), 226801 (2005).

[10] M. E. Cage, R. F. Dziuba, and B. F. Field, "A test of the quantum Hall effect as a resistance standard," IEEE Trans. Instrum. Meas. **IM–34**(2), 301–303 (1985).

[11] Y. Yin, M. Kruskopf, P. Gournay, B. Rolland, M. Götz, E. Pesel, T. Tschirner, D. Momeni, A. Chatterjee, F. Hohls, K. Pierz, H. Scherer, R. J. Haug, and H. W. Schumacher, "Graphene quantum Hall resistance standard for realizing the unit of electrical resistance under relaxed experimental conditions," Phys. Rev. Appl. **23**, 014025 (2025).

[12] N. Shetty, T. Bergsten, G. Eklund, S. L. Avila, S. Kubatkin, K. Cedergren, H. He, K. Cedergren, and H. H. Tan, "Long-term stability of molecular doped epigraphene quantum hall standards: Single elements and large arrays ($r_k/236 \approx 109\omega$)," Metrologia **60**, 055009 (2023).

[13] J. E. Avron, D. Osadchy, and R. Seiler, "A topological look at the quantum Hall effect," Phys. Today **56**(8), 38–42 (2003).

[14] Y. Hatsugai, "Topological aspects of the quantum Hall effect," J. Phys.: Condens. Matter **9**(12), 2507–2549 (1997).

[15] G. A. Baraff and D. C. Tsui, "Explanation of quantized-Hall-resistance plateaus in heterojunction inversion layers," Phys. Rev. B **24**, 2274 (1981).

[16] T. Toyoda, N. Hiraiwa, T. Fukuda, and H. Koizumi, "Plateaus in the dispersion of two-dimensional magnetoplasmons in GaAs quantum wells: Theoretical evidence of an electron reservoir," Phys. Rev. Lett. **100**, 036802 (2008).

[17] K. Yamada, T. Uchida, M. I. J. Fujita, and T. Toyoda, "The magnetic induction dependence of the quantum Hall resistivity of graphene two-dimensional electron system," Solid State Commun. **155**, 79 (2013).

[18] A. Groshev and G. Schön, "The width of the plateaus of the quantum Hall effect," Physica B **194–196**, 1249–1250 (1994).

[19] S. Kawaji, K. Hirakawa, and M. Nagata, "Device-width dependence of plateau width in quantum Hall states," Physica B **184**(1–4), 17–20 (1993).

[20] J. Schurr, J. Melcher, K. Pierz, G. Hein, and F.-J. Ahlers, "The width of AC quantum Hall plateaus," IEEE Trans. Instrum. Meas. **53**, 826–829 (2004).

[21] S. Yi-Thomas, Y. Huang, J. D. Sau, and S. Das Sarma, "Integer quantum Hall effect: Disorder, temperature, floating, and plateau width," Phys. Rev. B **111**, 195305 (2025).

[22] S. Datta, *Electronic Transport in Mesoscopic Systems* (Cambridge University Press, 1995).

[23] C. W. Groth, M. Wimmer, A. R. Akhmerov, and X. Waintal, "Kwant: A software package for quantum transport," New J. Phys. **16**(6), 063065 (2014).

[24] S. Lara-Avila, K. Moth-Poulsen, R. Yakimova, T. Bjørnholm, V. Fal'ko, A. Tzalenchuk, and S. Kubatkin, "Non-volatile photochemical gating of an epitaxial graphene/polymer heterostructure," Adv. Mater. **23**(7), 878–882 (2011).

[25] F. R. Bagsican, A. Winchester, S. Ghosh, X. Zhang, L. Ma, M. Wang, H. Murakami, S. Talapatra, R. Vajtai, P. M. Ajayan, J. Kono, M. Tonouchi, and I. Kawayama, "Adsorption energy of oxygen molecules on graphene and two-dimensional tungsten disulfide," Sci. Rep. **7**(1), 1774 (2017).

[26] H. Li, X. Han, A. S. Childress, A. M. Rao, and G. Koley, "Investigation of carrier density and mobility variations in graphene caused by surface adsorbates," Physica E **107**, 96–100 (2019).

[27] S. Ryu, L. Liu, S. Berciaud, Y.-J. Yu, H. Liu, P. Kim, G. W. Flynn, and L. E. Brus, "Atmospheric oxygen binding and hole doping in deformed graphene on a SiO_2 substrate," Nano Lett. **10**(12), 4944–4951 (2010).

[28] A. Lartsev, T. Yager, T. Bergsten, A. Tzalenchuk, T. J. B. M. Janssen, R. Yakimova, S. Lara-Avila, and S. Kubatkin, "Tuning carrier density across Dirac point in epitaxial graphene on SiC by corona discharge," Appl. Phys. Lett. **105**(6), 063106 (2014).

[29] Y. Yin, A. Chatterjee, D. Momeni, M. Kruskopf, M. Götz, S. Wundrack, F. Hohls, K. Pierz, and H. W. Schumacher, "Tailoring permanent charge carrier densities in epitaxial graphene on sic by functionalization with F4-TCNQ," Adv. Phys. Res. **1**(1), 2200015 (2022).

[30] X. Tian, J. Xu, and X. Wang, "Band gap opening of bilayer graphene by F4-TCNQ molecular doping and externally applied electric field," J. Phys. Chem. B **114**(35), 11377–11381 (2010).

[31] H. He, K. H. Kim, A. Danilov, D. Montemurro, L. Yu, Y. W. Park, F. Lombardi, T. Bauch, K. Moth-Poulsen, T. Iakimov, R. Yakimova, P. Malmberg, C. Müller, S. Kubatkin, and S. Lara-Avila, "Uniform doping of graphene close to the Dirac point by polymer-assisted assembly of molecular dopants," Nat. Commun. **9**(1), 3956 (2018).

[32] H. I. Wang, M.-L. Braatz, N. Richter, K.-J. Tielrooij, Z. Mics, H. Lu, N.-E. Weber, K. Müllen, D. Turchinovich, M. Kläui, and M. Bonn, "Reversible photochemical control of doping levels in supported graphene," J. Phys. Chem. C **121**(7), 4083–4091 (2017).

[33] A. Lherbier, B. Biel, Y.-M. Niquet, and S. Roche, "Transport length scales in disordered graphene-based materials: Strong localization regimes and dimensionality effects," Phys. Rev. Lett. **100**, 036803 (2008).

[34] A. Lherbier, X. Blase, Y.-M. Niquet, F. Triozon, and S. Roche, "Charge transport in chemically doped 2D graphene," Phys. Rev. Lett. **101**, 036808 (2008).

[35] J. H. Gosling, O. Makarovsky, F. Wang, N. D. Cottam, M. T. Greenaway, A. Patanè, R. D. Wildman, C. J. Tuck, L. Turyanska, and T. M. Fromhold, "Universal mobility characteristics of graphene originating from charge scattering by ionised impurities," Commun. Phys. **4**(1), 30 (2021).

[36] E. H. Hwang, S. Adam, and S. D. Sarma, "Carrier transport in two-dimensional graphene layers," Phys. Rev. Lett. **98**(18), 186806 (2007).

[37] K. Nomura and A. H. MacDonald, "Quantum transport of massless Dirac fermions," Phys. Rev. Lett. **98**(7), 076602 (2007).

[38] L. Turyanska, O. Makarovsky, L. Eaves, A. Patanè, and N. Mori, "Mobility enhancement of CVD graphene by spatially correlated charges," 2D Mater. **4**(2), 025026 (2017).

[39] O. Makarovsky, L. Turyanska, N. Mori, M. Greenaway, L. Eaves, A. Patané, M. Fromhold, S. Lara-Avila, S. Kubatkin, and R. Yakimova, "Enhancing optoelectronic properties of SiC-grown graphene by a surface layer of colloidal quantum dots," 2D Mater. **4**(3), 031001 (2017).

[40]C. J. Docherty, C.-T. Lin, H. J. Joyce, R. J. Nicholas, L. M. Herz, L.-J. Li, and M. B. Johnston, "Extreme sensitivity of graphene photoconductivity to environmental gases," Nat. Commun. **3**(1), 1228 (2012).
[41]F. Schedin, A. K. Geim, S. V. Morozov, E. W. Hill, P. Blake, M. I. Katsnelson, and K. S. Novoselov, "Detection of individual gas molecules adsorbed on graphene," Nat. Mater. **6**(9), 652–655 (2007).
[42]R. B. Laughlin, "Quantized Hall conductivity in two dimensions," Phys. Rev. B **23**(10), 5632–5633 (1981).
[43]P. Drude, "Zur elektronentheorie der metalle," Ann. Phys. **306**(3), 566–613 (1900).
[44]N. M. R. Peres, "*Colloquium*: The transport properties of graphene: An introduction," Rev. Mod. Phys. **82**, 2673–2700 (2010).
[45]M.-H. Liu, P. Rickhaus, P. Makk, E. Tóvári, R. Maurand, F. Tkatschenko, M. Weiss, C. Schönenberger, and K. Richter, "Scalable tight-binding model for graphene," Phys. Rev. Lett. **114**(3), 036601 (2015).
[46]S. Roche, N. Leconte, F. Ortmann, A. Lherbier, D. Soriano, and J.-C. Charlier, "Quantum transport in disordered graphene: A theoretical perspective," Solid State Commun. **152**(15), 1404–1410 (2012).
[47]P. M. Krstajić, "Integer quantum Hall effect in single-layer graphene with tilted magnetic field," J. Appl. Phys. **114**(7), 073705 (2013).
[48]T. P. Santos, L. R. F. Lima, and C. H. Lewenkopf, "An order *N* numerical method to efficiently calculate the transport properties of large systems: An algorithm optimized for sparse linear solvers," J. Comput. Phys. **394**, 440–455 (2019).